Simulation of cholesteric blue phases using a Landau–de Gennes theory: Effect of an applied electric field

Jun-ichi Fukuda（福田順一）,[1,2,*] Makoto Yoneya（米谷慎）,[1,2] and Hiroshi Yokoyama（横山浩）[1,2]
[1]*Nanotechnology Research Institute, National Institute of Advanced Industrial Science and Technology (AIST), 1-1-1 Umezono, Tsukuba 305-8568, Japan*
[2]*Liquid Crystal Nano-System Project, ERATO/SORST, Japan Science and Technology Agency, 5-9-9 Tokodai, Tsukuba 300-2635, Japan*
(Received 18 March 2009; published 15 September 2009)

We investigate numerically static and dynamic properties of cholesteric blue phases. Our study is based on a Landau–de Gennes theory describing the orientational order of a liquid crystal in terms of a second-rank tensor. To find the shape and size of the unit cell conforming to the minimum of the free energy, we let the geometrical parameters characterizing the unit cell relax in the course of the time evolution via a simple relaxational equation. We investigate the effect of an electric field on the structure of cholesteric blue phases. We study how the deformation of the unit cell in response to the electric field $\boldsymbol{E}$ depends on the strength and direction of the electric field and the original structure of cholesteric blue phases. Our results qualitatively agree with the experimental findings. Although in a weak field, the strain tensor is proportional to E^2 as previously argued, for a moderate field the distortion is no longer proportional to E^2 and can be even nonmonotonic with respect to E^2. Furthermore, we investigate the kinetic processes of the deformation, rearrangement, and extinction of disclination lines under a strong electric field. We show that the kinetics of disclination lines is highly complicated and sensitively depends on the initial structure of blue phases, the direction of the electric field, and the sign of dielectric anisotropy ϵ_a. In most cases, a strong field aligns the liquid crystals in a uniform (positive ϵ_a) or helical (negative ϵ_a) manner without disclination lines. However, for negative ϵ_a and the direction of the electric field parallel to the body diagonal of the unit cell, disclination lines do not disappear and form a two-dimensional hexagonal lattice.

DOI: 10.1103/PhysRevE.80.031706 PACS number(s): 61.30.Mp, 61.30.Gd, 61.30.Dk

I. INTRODUCTION

Cholesteric blue phases are intriguing examples of three-dimensional ordered structures of liquid crystals [1–6]. Blue phases are observed only in chiral liquid crystals, and their interesting features include Bragg scattering of light in the visible wavelength range, and the absence of birefringence (optically isotropic) in spite of the presence of Bragg scattering. For most of the liquid crystals exhibiting blue phases, three blue phases appear in a temperature range of a few K or less between an isotropic phase and a chiral nematic (cholesteric) phase. After extensive experimental [2,7–10] and theoretical [3,11–15] studies, most of which were carried out in the 1980s, those three phases are now identified as BP I possessing a body-centered-cubic structure [space group O_8 ($I4_132$)], BP II with a simple cubic structure [space group O_2 ($P4_232$)], and BP III believed to have an amorphous structure (BP III is beyond the scope of the present study; we restrict our attention to cubic BP I and BP II). In cubic BP I and BP II, cylinders made up of a "double twist" structure, which is favorable over a single helical twist locally, but is globally incompatible with topological requirements, are regularly stacked in a cubic manner separated by a network of disclination lines.

Early investigations of blue phases were triggered possibly by pure academic interest in the coexistence of Bragg scattering and optical isotropy; a very narrow temperature range in which blue phases are stable was considered to be a serious drawback for practical applications. However, a novel technique using photopolymerization was developed recently to extend the temperature range of the stability of blue phases (polymer-stabilized blue phases) [16], and new compounds exhibiting blue phases stable in a temperature range of as large as 40–50 K were discovered [17]. Due to those successful attempts to stabilize blue phases in a wide temperature range, blue phases have been attracting greater interest from the viewpoint of possible applications, including lasers [18,19] and displays [20]. For the success of practical applications of blue phases, theoretical understanding of the dynamics as well as statics of blue phases in response to external perturbations such as an electric field is desirable and necessary.

Many of the previous theoretical studies on cubic blue phases [3,13–15] are based on a Landau–de Gennes theory [21], in which the local orientational order of a liquid crystal is described by a second-rank symmetric and traceless tensor $Q_{\alpha\beta}$. Analytical studies have been carried out using mode expansions of $Q_{\alpha\beta}$ to investigate the stability of possible candidate structures of blue phases and the response of blue phase structures to an electric field. Although those analytical studies succeed in explaining general properties of cubic blue phases, some of the experimental findings, for example, the deformation of the unit cell of BP I in response to an applied electric field (anomalous electrostriction), are incompatible with the results of those theories. Therefore, numerical studies that do not rely on mode expansions should be greatly motivated. We also note that the use of a tensor order

*fukuda.jun-ichi@aist.go.jp

parameter has a numerical advantage; in contrast to the director ($\boldsymbol{n}$) description [12], topological defects, or disclination lines, inherent in blue phases do not have to be treated separately as singularities. However, there have only a few numerical studies on cholesteric blue phases [22–25], all of which are based on lattice-Boltzmann method.

In this paper, we present our numerical attempts to investigate the statics and dynamics of cholesteric blue phases. One of the difficulties in the simulations of three-dimensional structures, including blue phases, is that the mismatch between the characteristic size of the structures one wants to simulate and the size of the numerical system should be avoided. The rescaling factor to avoid this mismatch is referred to as a "redshift" (precisely, redshift implies the ratio of the characteristic wave number of the cubic blue phases to that of a helical alignment in previous theoretical studies [3,13–15]). In Ref. [22], a fixed value of the redshift taken from the previous literature was employed. In Ref. [23], the value of the redshift was calculated at each iteration. In our study, we take the redshift into account by relaxing the size and shape of the numerical system in the course of the time evolution. This is achieved by assuming the relaxational equations for the parameters characterizing the size and shape of the numerical system. It is not yet clear how simultaneous changes in the order parameter $Q_{\alpha\beta}$ and the shape of the unit cell should be incorporated in simulations. Our present attempt can be one candidate.

Our main goal in the present paper is to study the effect of an applied electric field on the structure of cubic blue phases. The understanding of the response of blue phases to an applied field is not only of fundamental interest but also highly important in practical applications. Although a number of experimental [6,26–32] and theoretical attempts [33–36] have been carried out to understand the properties of blue phases under an applied field, so far as we know, there has been only one numerical study focusing on the effect of an electric field on blue phases [24]. Reference [24] is a short contribution, paying attention to the cases with positive dielectric anisotropy; negative dielectric anisotropy is beyond its scope. Moreover, its main concern is the cases in which the field is applied along one side of the unit cell; other cases are only very briefly discussed. Although it considers the reorganization of disclination lines under a relatively strong field, only a small number of results are shown. In the present paper, we carry out extensive studies to check how the response of blue phases depends on the strength and direction of the electric field, the sign of the dielectric anisotropy, and the original blue phase structures [BP I (O_8) or BP II (O_2)]. We also present the kinetic process of reorganization and extinction of disclination lines under a strong field for various cases.

In Sec. II, we describe the details of the Landau–de Gennes theory and its numerical implementation. Our numerical results are given in Sec. III. Section IV concludes this paper.

II. MODEL

A. Order parameter and free-energy density

As noted in the introduction, the orientational order of a liquid crystal is described by a second-rank symmetric and traceless tensor $Q_{\alpha\beta}$ in a Landau–de Gennes theory. The free-energy density of a chiral liquid crystal [5] is given by $f = f_{\mathrm{local}}\{Q_{\alpha\beta}\} + f_{\mathrm{grad}}\{Q_{\alpha\beta}, \nabla\} + f_E\{Q_{\alpha\beta}, \boldsymbol{E}\}$, in which

$$f_{\mathrm{local}}\{Q_{\alpha\beta}\} = c\ \mathrm{Tr}\ \mathbf{Q}^2 - \sqrt{6}b\ \mathrm{Tr}\ \mathbf{Q}^3 + a(\mathrm{Tr}\ \mathbf{Q}^2)^2 \tag{1}$$

is the local free energy in the Landau–de Gennes expansion,

$$f_{\mathrm{grad}}\{Q_{\alpha\beta}, \nabla\} = \frac{1}{4}K_1[(\nabla \times \mathbf{Q})_{\alpha\beta} + 2q_0 Q_{\alpha\beta}]^2 + \frac{1}{4}K_0[(\nabla \cdot \mathbf{Q})_\alpha]^2 \tag{2}$$

is the free energy due to the inhomogeneity of liquid crystalline order, and

$$f_E = -\bar{\epsilon}_{\mathrm{a}} E_\alpha E_\beta Q_{\alpha\beta} \tag{3}$$

is the energy due to the electric field. In f_{local}, a and b are positive constants and c is assumed to vary with temperature. In Eqs. (2) and (3), summations over repeated indices are implied, $(\nabla \times \mathbf{Q})_{\alpha\beta} \equiv \epsilon_{\alpha\gamma\delta}\nabla_\gamma Q_{\delta\beta}$, and $(\nabla \cdot \mathbf{Q})_\alpha \equiv \nabla_\beta Q_{\beta\alpha}$, with $\epsilon_{\alpha\gamma\delta}$ being the Levi-Civita symbol. The variables K_1 and K_0 are the elastic constants, and q_0 characterizes the strength and sign of the chirality of the liquid crystal (hereafter, we consider the case with $q_0 > 0$) and is related to the pitch of a cholesteric helix. The dielectric anisotropy is represented by $\bar{\epsilon}_{\mathrm{a}}$ (hereafter, we omit the overline of $\bar{\epsilon}_{\mathrm{a}}$ if only the sign of the dielectric anisotropy is of interest). We also note that following the spirit of the Landau expansion, we assume that the temperature dependence appears only in the parameter c and neglect the temperature dependence of the other material parameters.

After an appropriate rescaling of the variables, we can reduce the number of relevant parameters. Here we follow the rescaling of Wright and Mermin [5] and the rescaled free-energy density $\varphi \equiv (a^3/b^4)f$ is written, in terms of a rescaled tensor order parameter $\chi_{\alpha\beta} \equiv (a/b)Q_{\alpha\beta}$ and a rescaled spatial derivative $\tilde{\nabla} \equiv (2q_0)^{-1}\nabla$, as $\varphi = \varphi_{\mathrm{local}}\{\chi_{\alpha\beta}\} + \varphi_{\mathrm{grad}}\{\chi_{\alpha\beta}, \tilde{\nabla}\} + \varphi_E\{\chi_{\alpha\beta}, \boldsymbol{E}\}$, where

$$\varphi_{\mathrm{local}}\{\chi_{\alpha\beta}\} = \tau\ \mathrm{Tr}\ \chi^2 - \sqrt{6}\ \mathrm{Tr}\ \chi^3 + (\mathrm{Tr}\ \chi^2)^2, \tag{4}$$

$$\varphi_{\mathrm{grad}}\{\chi_{\alpha\beta}, \tilde{\nabla}\} = \kappa^2\{[(\tilde{\nabla} \times \chi)_{\alpha\beta} + \chi_{\alpha\beta}]^2 + \eta[(\tilde{\nabla} \cdot \chi)_\alpha]^2\}, \tag{5}$$

$$\varphi_E\{\chi_{\alpha\beta}, \boldsymbol{E}\} = -\tilde{\epsilon}\hat{e}_\alpha\hat{e}_\beta\chi_{\alpha\beta}. \tag{6}$$

Here $\tau \equiv (a/b^2)c$ is related to temperature, and $\kappa \equiv \sqrt{aK_1q_0^2/b^2}$ is a rescaled chirality. The parameter $\eta \equiv K_0/K_1$ concerns the anisotropy of elasticity, and hereafter just for simplicity we set $\eta = 1$ (so-called one-constant approximation). Concerning φ_E, we have defined a unit vector specifying the direction of $\boldsymbol{E}$, that is, $\hat{\boldsymbol{e}} \equiv \boldsymbol{E}/|\boldsymbol{E}|$, and the rescaled strength of the field [34],

$$\tilde{\epsilon} \equiv (a^2/b^3)\bar{\epsilon}_{\mathrm{a}}E^2. \tag{7}$$

Here we implicitly assume, just for simplicity, that the electric field $\boldsymbol{E}$ is uniform and fixed throughout the system, although $\boldsymbol{E}$ can be nonuniform due to the inhomogeneity in the dielectric tensor arising from nonuniform alignment of the liquid crystal.

We note that in the Landau–de Gennes expansion, the prefactor of Tr χ^2 corresponds to the (rescaled) temperature. The term Tr χ^2 appears not only in φ_{local} but also in φ_{grad}, and therefore $\tau+\kappa^2$ rather than τ should be considered as representing the rescaled temperature. It should be also mentioned that $\tilde{\epsilon}$ can be positive or negative depending on the sign of the dielectric anisotropy ϵ_a. Hereafter, length is measured in units of $(2q_0)^{-1}$ and we omit the tilde in $\tilde{\nabla}$.

B. Numerical implementation and relaxation of the system

In our numerical calculations, we use $N\times N\times N$ grids with periodic boundary conditions and $N=32$ to accommodate a unit cell of cholesteric blue phases. The order parameter $\chi_{\alpha\beta}$ is assigned at each grid point. To specify the grid points, we introduce a set of integer variables $\{\xi_l\}$ with $l=1$, 2, 3, and ξ_l varies from 0 to $N-1$. The position of the grid point at $\{\xi_l\}$ in real space is given by $\boldsymbol{r}=\Sigma_{l=1}^{3}(\partial\boldsymbol{r}/\partial\xi_l)\xi_l$. Here $\boldsymbol{r}=(r_1,r_2,r_3)$ or (x,y,z). The vector $\partial\boldsymbol{r}/\partial\xi_l$ is not allowed to vary with respect to $\{\xi_l\}$, so that the sides of our unit cell are straight lines and the shape of our unit cell is in general a parallelepiped (it is of course a cube when no external field is applied). However, to account for the "redshift" in determining the equilibrium structure of blue phases (under no external field), or the distortion of the unit cell due to the applied electric field, we let $\partial\boldsymbol{r}/\partial\xi_l$ vary with time in the course of relaxation. How to let $\partial\boldsymbol{r}/\partial\xi_l$ evolve with time will be described later.

To describe the time evolution of the order parameter $\chi_{\alpha\beta}$, we use a simplified relaxation equation

$$\tau_\chi\frac{\partial}{\partial t}\chi_{\alpha\beta}(\boldsymbol{r})=-\left[\frac{\delta\mathcal{F}}{\delta\chi_{\alpha\beta}(\boldsymbol{r})}-\lambda\delta_{\alpha\beta}(\boldsymbol{r})\right], \tag{8}$$

where $\mathcal{F}$ is the total free energy of the system, τ_χ is the characteristic time of the relaxation proportional to the rotational viscosity, and λ is the Lagrange multiplier ensuring Tr $\chi=\chi_{\alpha\alpha}=0$. Although several previous numerical studies concerning cholesteric blue phases [24,25] took into account hydrodynamics, we do not do so in our study because it is quite difficult to incorporate the hydrodynamic flow together with the simultaneous change in the shape of the unit cell (to our knowledge, none of the previous studies concerning liquid crystals have succeeded in, nor paid attention to, taking into account the hydrodynamic flow and the change in the shape of the numerical lattice system simultaneously). We also note that by choosing material parameters $\gamma_1\simeq 0.1$ Pa s (rotational viscosity in Ericksen-Leslie equations), $K\simeq 10$ pN (Frank elastic constant in the director description), and $q_0\simeq 5\times 10^7$ m^{-1}, and $\kappa=0.7$ (which is employed in the simulations below), the characteristic time τ_χ is estimated as $\tau_\chi\simeq 1$ μs.

To evaluate the functional derivative $\delta\mathcal{F}/\delta\chi_{\alpha\beta}$ in the discretized space, we use the procedure similar to that employed in Ref. [37]. The detail of the evaluation is given in Appendix A. The left-hand side of Eq. (8) is discretized using an explicit Euler scheme. We let the time increment Δt vary in response to the change in the shape and the size of the system with the variation of $\partial\boldsymbol{r}/\partial\xi_l$. How to choose Δt will be given later.

Here we describe how to let $\partial\boldsymbol{r}/\partial\xi_l$, or the size and shape of the unit cell, evolve with time. When we intend to obtain the true equilibrium profile of our system, we have to minimize the free-energy density of the whole system, which we will denote by $\bar{\varphi}$, with respect to the variation in the size and shape of the unit cell, as well as with respect to the variation of $\chi_{\alpha\beta}$. We again use a simple form of the relaxation equation

$$\tau_\Delta\frac{\partial}{\partial t}\frac{\partial\xi_i}{\partial r_j}=-\frac{\partial}{\partial(\partial\xi_i/\partial r_j)}\bar{\varphi}. \tag{9}$$

Using the notations in Appendix A, we can express $\bar{\varphi}$ as

$$\bar{\varphi}=\frac{\mathcal{F}}{V}=\frac{1}{N^3}\sum_{i=0}^{N-1}\sum_{j=0}^{N-1}\sum_{k=0}^{N-1}\varphi_{\text{voxel}}(i,j,k), \tag{10}$$

where $V=N^3v_{\text{voxel}}$ is the volume of our system. We notice that the free-energy density in a simulation voxel $\varphi_{\text{voxel}}(i,j,k)$ depends on $\partial\xi_l/\partial r_k$, as noted in Appendix A. Note also that the tensor $\partial\xi_l/\partial r_k$ is obtained by calculating the inverse of $\partial\boldsymbol{r}/\partial\xi_l$.

At present, we have no idea how to relate the characteristic time τ_Δ for the deformation of the unit cell with material parameters such as a rotational viscosity or other kinetic coefficients. Here we choose $\tau_\Delta=0.305\tau_\chi$, but we do not have any reason for this specific choice. When one is interested in the equilibrium structures of blue phases, in particular, in the dimension of the unit cell of some specific blue phase structures as we will discuss below, the choice of τ_Δ is not important, unless numerical instabilities occur. However, kinetic pathways toward the equilibrium structures might be significantly influenced by the choice of τ_Δ. In the following, we will present the results of not only the equilibrium structures of blue phases but also the kinetic process of the deformation of disclination lines under an applied electric field, with the belief that even with one choice of τ_Δ, our numerical results will shed light on possible kinetics of blue phases under an external field.

Finally, we mention how we choose the time increment Δt. When we pick up the second-order terms in the derivatives in Eq. (8), we have a simple diffusion equation $\tau_\chi(\partial/\partial t)\chi_{\alpha\beta}=2\kappa^2\nabla^2\chi_{\alpha\beta}$. In a cubic mesh with mesh spacing Δx, for the discretized version of this diffusion equations to be stable in an Euler scheme, the time increment must satisfy $\Delta t\le(1/6)\Delta x^2/(2\kappa^2)$ [38]. With this fact in mind, We choose Δt in our simulations as $\Delta t=0.05\Delta_{\text{min}}^2/(2\kappa^2)$ with $\Delta_{\text{min}}=\min_{l=1,2,3}\{|\partial\boldsymbol{r}/\partial\xi_i|\}$. We choose the prefactor 0.05 just to ensure the stability of the calculation. We also note that when the grids expand so much that $|\partial\boldsymbol{r}/\partial\xi_i|$ becomes large, Δt also becomes large to induce instability due to other contributions in the right-hand side of Eq. (8). Therefore, when Δt determined by above exceeds 0.02, we reset Δt to 0.02.

III. RESULTS

In this section, we present our numerical results to demonstrate how the unit cell deforms and the disclination lines are distorted in response to the applied electric field. We restrict our attention to the phases O_8^- (BP I) and O_2 (BP II).

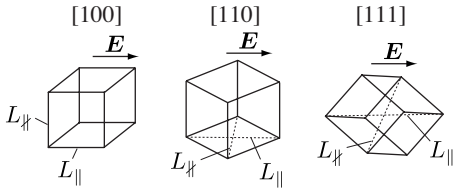

FIG. 1. Illustration of the definitions of $L_{\parallel}$ and $L_{\nparallel}$ for the cases with $\boldsymbol{E}$ parallel to the [100], [110], and [111] directions.

We choose the parameters $\kappa=0.7$ and $\tau=-1$ for O_8^-, and $\kappa=0.7$ and $\tau=-0.3$ for O_2. We have checked that for $\kappa=0.7$ and under no external field, O_8^- and O_2 structures are indeed the most stable at $\tau=-1$ and -0.3, respectively. In the following numerical calculations, equilibrium order-parameter profiles of O_8^- ($\kappa=0.7$ and $\tau=-1$) and O_2 ($\kappa=0.7$ and $\tau=-0.3$) structures under no external field are used as initial conditions.

Before presenting our results, we note that the relation between $\tilde{\epsilon}$ defined in Eq. (7) and the strength of the electric field $\boldsymbol{E}$ in units of V/μm is given by

$$|\tilde{\epsilon}| \simeq 2 \times 10^{-3} E^2. \tag{11}$$

The derivation of Eq. (11) is given in Appendix B. A field $E=1$ V/μm, which is considered to be weak enough in previous experiments [30], corresponds to $|\tilde{\epsilon}| \simeq 0.002$. The choice of $|\tilde{\epsilon}|=5$ in Sec. III B discussing the effect of a strong field is equivalent to $E \simeq 50$ V/μm.

A. Deformation of a unit cell in a weak and moderate field

Here we show the results of the deformation of the unit cell under the application of an electric field. How the unit cell is distorted in response to the electric field depends on not only the structure of blue phases (O_8^- or O_2) but also on the direction of the electric field with respect to the unit cell. Therefore, we denote the directions of the sides of the undistorted unit cell by x, y, and z directions and consider the cases where the applied field $\boldsymbol{E}$ is along the $\boldsymbol{e}_x$, or [100], direction, the $\boldsymbol{e}_x+\boldsymbol{e}_y$, or [110], direction, and the $\boldsymbol{e}_x+\boldsymbol{e}_y+\boldsymbol{e}_z$, or [111], direction. To quantify the deformation of the unit cell, we define the characteristic lengths of the unit cell along and not along the electric field $L_{\parallel}$ and $L_{\nparallel}$, as illustrated in Fig. 1; in the case of $\boldsymbol{E}\|[100]$, $L_{\parallel}$ is the length of a side of the unit cell parallel to $\boldsymbol{E}$, and $L_{\nparallel}$ is that of a side perpendicular to $\boldsymbol{E}$. When $\boldsymbol{E}\|[110]$, $L_{\parallel}$ is the length of a face diagonal parallel to $\boldsymbol{E}$, and $L_{\nparallel}$ is that of a face diagonal perpendicular to $\boldsymbol{E}$. In the case of $\boldsymbol{E}\|[111]$, $L_{\parallel}$ is the length of a body diagonal parallel to $\boldsymbol{E}$, and $L_{\parallel}$ is the length of a body diagonal not parallel to $\boldsymbol{E}$ (we note that due to the threefold symmetry about the [111] axis, the lengths of three body diagonals not parallel to $\boldsymbol{E}$ are equal).

Before presenting our results, we notice that previous literature [6,27,30,35,36] summarized their results using the fact that, in the case of a weak electric field, the deformation of the unit cell is proportional to the square of the field strength and can be expressed in terms of the electrostriction tensor $\boldsymbol{R}$. After defining the symmetric deformation tensor $u_{ij}=\frac{1}{2}(\partial_i u_j+\partial_j u_i)$, with the vector $\boldsymbol{u}$ characterizing the shift of lattice points under the deformation, the electrostriction tensor $\boldsymbol{R}$ is given by

$$u_{ij} = R_{ijkl} E_k E_l, \tag{12}$$

where summations over repeated indices are implied. Due to the cubic symmetry of the undistorted blue phases, the electrostriction tensor $\boldsymbol{R}$ has only three independent components, namely, $R_1=R_{xxxx}$, $R_2=R_{xxyy}$, and $R_3=2R_{yzyz}$. In the regime of linear elasticity with Eq. (12), the above definitions of $L_{\parallel}$ and $L_{\nparallel}$ lead to

$$2R_1E^2 = \frac{L_{\parallel}^2 - L_0^2}{L_0^2}, \quad 2R_2E^2 = \frac{L_{\nparallel}^2 - L_0^2}{L_0^2}, \tag{13}$$

for $\boldsymbol{E}\|[100]$, where L_0 is the dimension of the undistorted cubic unit cell,

$$R_3E^2 = \frac{L_{\parallel}^2 - L_{\nparallel}^2}{(\sqrt{2}L_0)^2}, \tag{14}$$

for $\boldsymbol{E}\|[110]$, and

$$\frac{8}{9}R_3E^2 = \frac{L_{\parallel}^2 - L_{\nparallel}^2}{(\sqrt{3}L_0)^2}, \tag{15}$$

for $\boldsymbol{E}\|[111]$. The derivation of Eqs. (13)–(15) is given in Appendix C. Equations (14) and (15) can be used to check if the deformation of the unit cell under an electric field can indeed be described by Eq. (12).

Figure 2 shows the distortions of the unit cell with respect to $\tilde{\epsilon}$, when the field is applied along the [100] direction. Recall, from the definition of $\tilde{\epsilon}$ in Eq. (7), that the sign of the dielectric anisotropy ϵ_a determines that of $\tilde{\epsilon}$ and that $\tilde{\epsilon}$ is proportional to E^2. Therefore, when linear elasticity and Eq. (12) hold, it is expected that the graphs in Fig. 2 become linear passing through the origin. This is indeed the case, as can be seen from Figs. 2(b) and 2(d).

We find from Fig. 2 that when the dielectric anisotropy is positive, that is, $\tilde{\epsilon}>0$, the O_8^- unit cell shrinks along the field direction ($L_{\parallel}<L_{\nparallel}$), and that the O_2 unit cell expands along the field direction ($L_{\parallel}>L_{\nparallel}$). Vice versa for $\tilde{\epsilon}<0$. In other words, the O_8^- structure gives, in the case of a sufficiently weak electric field, $R_1<0$ and $R_2>0$ for positive dielectric anisotropy, and $R_1>0$ and $R_2<0$ for negative dielectric anisotropy. The O_2 structure results in $R_1>0$ and $R_2<0$ for positive dielectric anisotropy, and $R_1<0$ and $R_2>0$ for negative dielectric anisotropy. These results agree qualitatively with previous experimental [6,30] and numerical [24] findings. In Table I, we give the values of the rescaled components of the electrostriction tensor $R_i/(a^2/b^3)|\bar{\epsilon}_a|$, with $i=1,2$, calculated using our results for $|\tilde{\epsilon}|=0.001$ together with Eq. (13). We note that $(a^2/b^3)|\bar{\epsilon}_a| \simeq 2\times10^{-15}$ m^2/V^{-2} (see Appendix B), which leads to the values of the dimensional R_1 and R_2 on the order of 10^{-15} m^2/V^{-2}. This agrees with the experimental findings, which gives $R \simeq 10^{-14}-10^{-15}$ m^2/V^{-2} [6,27,30]. We also note that for both cases of O_8^- and O_2, $R_1 \simeq -2R_2$ holds well, which implies the conservation of the volume of the unit cell [35]. In previous experiments, volume conservation of the unit cell of blue phases under a weak electric field has been observed [30],

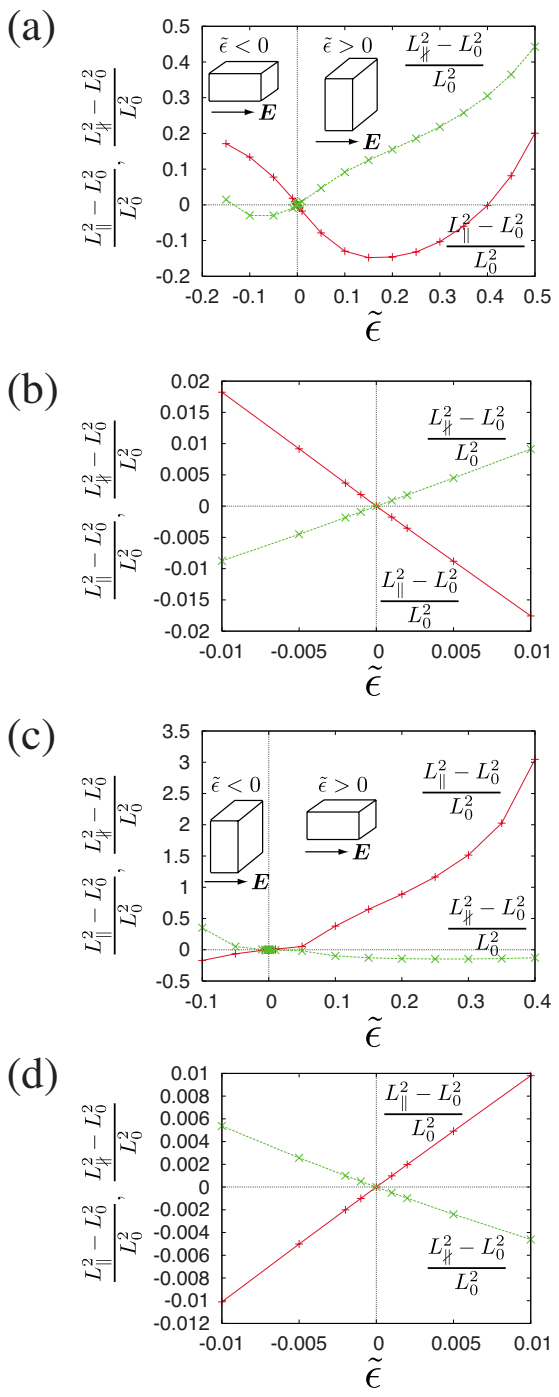

FIG. 2. (Color online) Plots of $(L_{\parallel}^2-L_0^2)/L_0^2$ and $(L_{\nparallel}^2-L_0^2)/L_0^2$ for (a) and (b) O_8^- and (c) and (d) O_2 structures, when the field is applied along the [100] direction. (b) and (d) are magnified plots of (a) and (c), respectively, for small $|\tilde{\epsilon}|$. Solid lines with + symbols (red) represent $(L_{\parallel}^2-L_0^2)/L_0^2$, and dashed lines with × symbols (green) represent $(L_{\nparallel}^2-L_0^2)/L_0^2$.

although a relation which does not support volume conservation for the O_2 blue phase ($R_1 \simeq -2.6R_2$) has also been reported [27].

We also note the nonlinear behavior of $(L_{\parallel}^2-L_0^2)/L_0^2$, and $(L_{\nparallel}^2-L_0^2)/L_0^2$, which clearly indicates that linear elasticity and Eq. (12) hold only in a very small range of $\tilde{\epsilon}$ around $\tilde{\epsilon}=0$. In the O_8^- case, we even see nonmonotonic behavior of $(L_{\parallel}^2-L_0^2)/L_0^2$, and $(L_{\nparallel}^2-L_0^2)/L_0^2$, with respect to $\tilde{\epsilon}$, although $L_{\nparallel}>L_{\parallel}$ and $L_{\nparallel}<L_{\parallel}$ are always satisfied for $\tilde{\epsilon}>0$ and $\tilde{\epsilon}<0$, respectively.

TABLE I. The rescaled values of the coefficients of the electrostriction tensor $R_i/(a^2/b^3)|\bar{\epsilon}_a|$ with $i=1,2$.

		$R_1/(a^2/b^3)\lvert\bar{\epsilon}_a\rvert$	$R_2/(a^2/b^3)\lvert\bar{\epsilon}_a\rvert$
O_8^-	$\epsilon_a>0$	−0.883	0.442
	$\epsilon_a<0$	0.920	−0.460
O_2	$\epsilon_a>0$	0.493	−0.249
	$\epsilon_a<0$	−0.501	0.249

In Fig. 3, we show the plots of $(L_{\parallel}^2-L_0^2)/(\sqrt{2}L_0)^2$ for $\boldsymbol{E}\|[110]$ and $(L_{\parallel}^2-L_0^2)/(\sqrt{3}L_0)^2$ for $\boldsymbol{E}\|[111]$ with the variation of $\tilde{\epsilon}$. When $|\tilde{\epsilon}|$ is small, we find, from Figs. 3(b) and 3(d) [Eqs. (14) and (15)], that $R_3>0$ (or expansion along the field direction) for positive dielectric anisotropy ($\tilde{\epsilon}>0$), and $R_3<0$ (expansion perpendicular to the field direction) for negative dielectric anisotropy ($\tilde{\epsilon}<0$) for both O_8^- and O_2 structures, reproducing qualitatively the previous experimental findings for $\boldsymbol{E}\|[110]$. For small $|\tilde{\epsilon}|$, we again observe in Figs. 3(b) and 3(d) the behavior of the distortions linear in $\tilde{\epsilon}$. However, Figs. 3(a) and 3(c) show that in principle $(L_{\parallel}^2-L_0^2)/(\sqrt{2}L_0)^2$ and $(L_{\parallel}^2-L_0^2)/(\sqrt{3}L_0)^2$ do not depend linearly on ϵ, again indicating that linear elasticity and Eq. (12) hold only in a very small range of $\tilde{\epsilon}$ around $\tilde{\epsilon}=0$. Moreover, for positive $\tilde{\epsilon}$, $L_{\parallel}^2-L_{\nparallel}^2$ for O_2 with $\boldsymbol{E}\|[110]$ and $\boldsymbol{E}\|[111]$ changes sign at $\tilde{\epsilon}\simeq 0.12$ and $\tilde{\epsilon}\simeq 0.22$, respectively. This behavior gives another example of a nontrivial response of blue phases to an applied electric field.

Finally, we summarize in Table II the values of the rescaled component of the electrostriction tensor $R_3/(a^2/b^3)|\bar{\epsilon}_a|$ deduced from our calculation results with $|\tilde{\epsilon}|=0.001$ using Eqs. (14) and (15). If linear elasticity and Eq. (12) hold, it should be expected that the value of R_3 should be the same irrespective of the direction of the electric field $\boldsymbol{E}$. We find from Table II that the results for different field direction ([110] and [111]) give almost the same values of R_3, indicating the validity of linear elasticity and Eq. (12) for a sufficiently weak field.

B. Distortion of disclination lines in a strong field

In the previous section (Sec. III A), we restricted our discussions to the effect of a relatively weak electric field and investigated how the unit cell is deformed due to the applied field. Here we consider the cases where a strong field is applied to blue phases and observe how the disclination lines are distorted under the influence of an electric field. We set the rescaled field strength to $|\tilde{\epsilon}|=5$ and again consider the cases where the field is along the [100], [110], or [111] direction. Under a strong field, it is expected that when the dielectric anisotropy is positive, i.e., $\tilde{\epsilon}>0$, the liquid crystals are aligned uniformly along the field, while with a negative dielectric anisotropy ($\tilde{\epsilon}<0$), helical alignment whose helical axis is along the field is achieved. Therefore, we will inves-

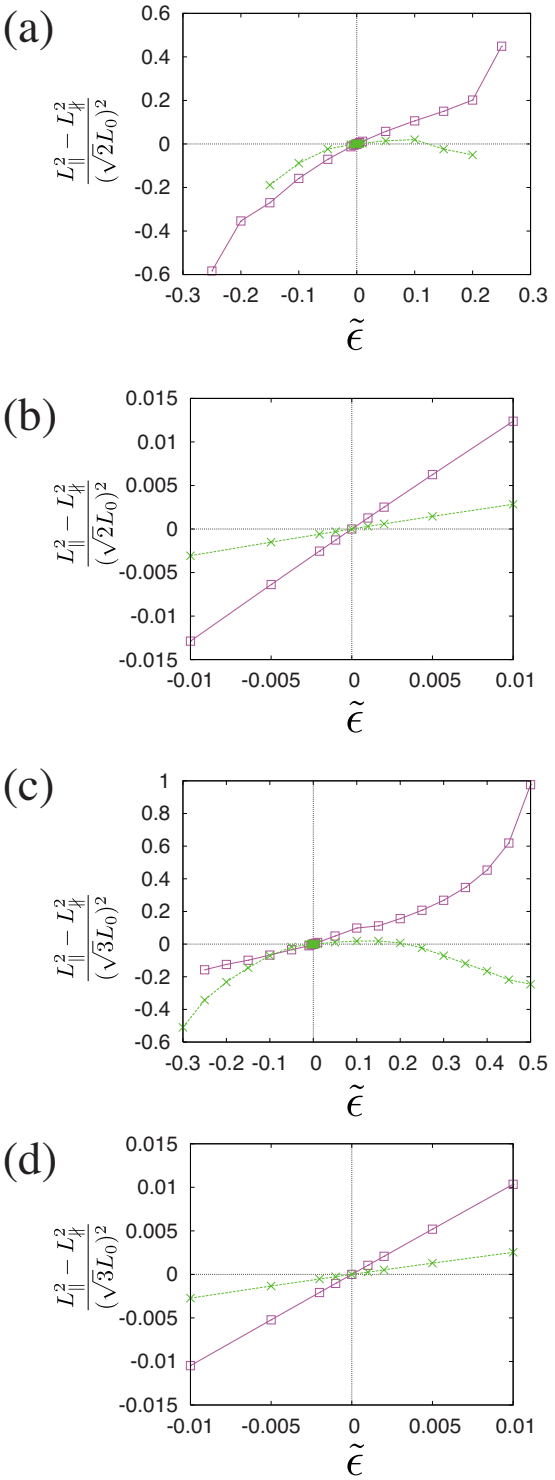

FIG. 3. (Color online) Plots of (a) and (b) $(L_\parallel^2 - L_0^2)/(\sqrt{2}L_0)^2$ for $\boldsymbol{E}\|[110]$ and (c) and (d) $(L_\parallel^2 - L_0^2)/(\sqrt{3}L_0)^2$ for $\boldsymbol{E}\|[111]$. (b) and (d) are magnified plots of (a) and (c), respectively, for small $|\tilde{\epsilon}|$. Solid lines with square (□) symbols (magenta) and dashed lines with cross (×) symbols (green) represent the results for O_8^- and O_2 structures, respectively.

tigate whether such uniform or helical alignment is indeed realized after a sufficiently long time, and if so, what kinetic processes the system experiences before reaching such alignment.

TABLE II. The rescaled values of the coefficient of the electrostriction tensor $R_3/(a^2/b^3)|\bar{\epsilon}_a|$.

			$R_3/(a^2/b^3)\lvert\bar{\epsilon}_a\rvert$
O_8^-	$\epsilon_a>0$	$\boldsymbol{E}\|[110]$	1.261
		$\boldsymbol{E}\|[111]$	1.171
	$\epsilon_a<0$	$\boldsymbol{E}\|[110]$	−1.265
		$\boldsymbol{E}\|[111]$	−1.171
O_2^-	$\epsilon_a>0$	$\boldsymbol{E}\|[110]$	0.297
		$\boldsymbol{E}\|[111]$	0.295
	$\epsilon_a<0$	$\boldsymbol{E}\|[110]$	−0.297
		$\boldsymbol{E}\|[111]$	−0.300

In Figs. 4–9, we show the time evolution of the equilibrium O_8 (Figs. 4, 6, and 8) and O_2 (Figs. 5, 7, and 9) structures after the application of the electric field. As noted above, the field direction is along the [100] (Figs. 4 and 5), [110] (Figs. 6 and 7), or [111] (Figs. 8 and 9) direction. In each figure, the cases with positive and negative dielectric anisotropies, i.e., $\tilde{\epsilon}=5$ and −5 are presented in (a) and (b), respectively. We also notice that, unless otherwise stated in the figure captions, the viewpoint of the figure stays unchanged throughout the time evolution. Therefore, the change in the size and shape of the unit cell is correctly presented in Figs. 4–9.

From Figs. 4–7, we find that the O_8^- and O_2 blue phases under an electric field along the [100] or [110] direction indeed relax to a uniformly aligned state (positive dielectric anisotropy) or a helical state (negative dielectric anisotropy) without disclination lines, via a complicated process of the reorganization and extinction of disclination lines. It is interesting to see winding of disclination lines in the O_8^- cases (Figs. 4 and 6), which can be obviously seen in Fig. 6(a) at $\tau=0.396$. In the case of the field along the [100] direction (Fig. 4), curled disclination lines are reconnected to form disclination rings and those disclination rings shrink and disappear for the overall orientational profile to become uniform or helical. We also note the strong deformation of the unit cell when an electric field is applied along the [110] direction to the O_8^- phase with negative dielectric anisotropy [Fig. 6(b)]. In the O_2 cases, the initial junction of four disclination lines disappears immediately after the application of the electric field to form two nonconnected disclination lines. After that various kinetic processes are found depending on the direction of the electric field and the sign of the dielectric anisotropy; the change in the folding direction of the disclination lines [Fig. 5(a): $\boldsymbol{E}\|[100]$, positive $\tilde{\epsilon}$], creation of new disclination lines [Fig. 5(b) at $t/\tau_\chi=0.412$: $\boldsymbol{E}\|[100]$, negative $\tilde{\epsilon}$], winding of the disclination lines and formation of a disclination ring [Fig. 7(a): $\boldsymbol{E}\|[110]$, positive $\tilde{\epsilon}$], and reconnection and topological change in disclination lines [Fig. 7(b): $\boldsymbol{E}\|[110]$, negative $\tilde{\epsilon}$] are observed.

Different kinetic pathways are seen when the field is along the [111] direction. We note that both the O_8^- and O_2 structures have one disclination line parallel to the [111] direction, while no disclination lines are along the [100] or [110] direction. In the cases of positive $\tilde{\epsilon}$, the disclination

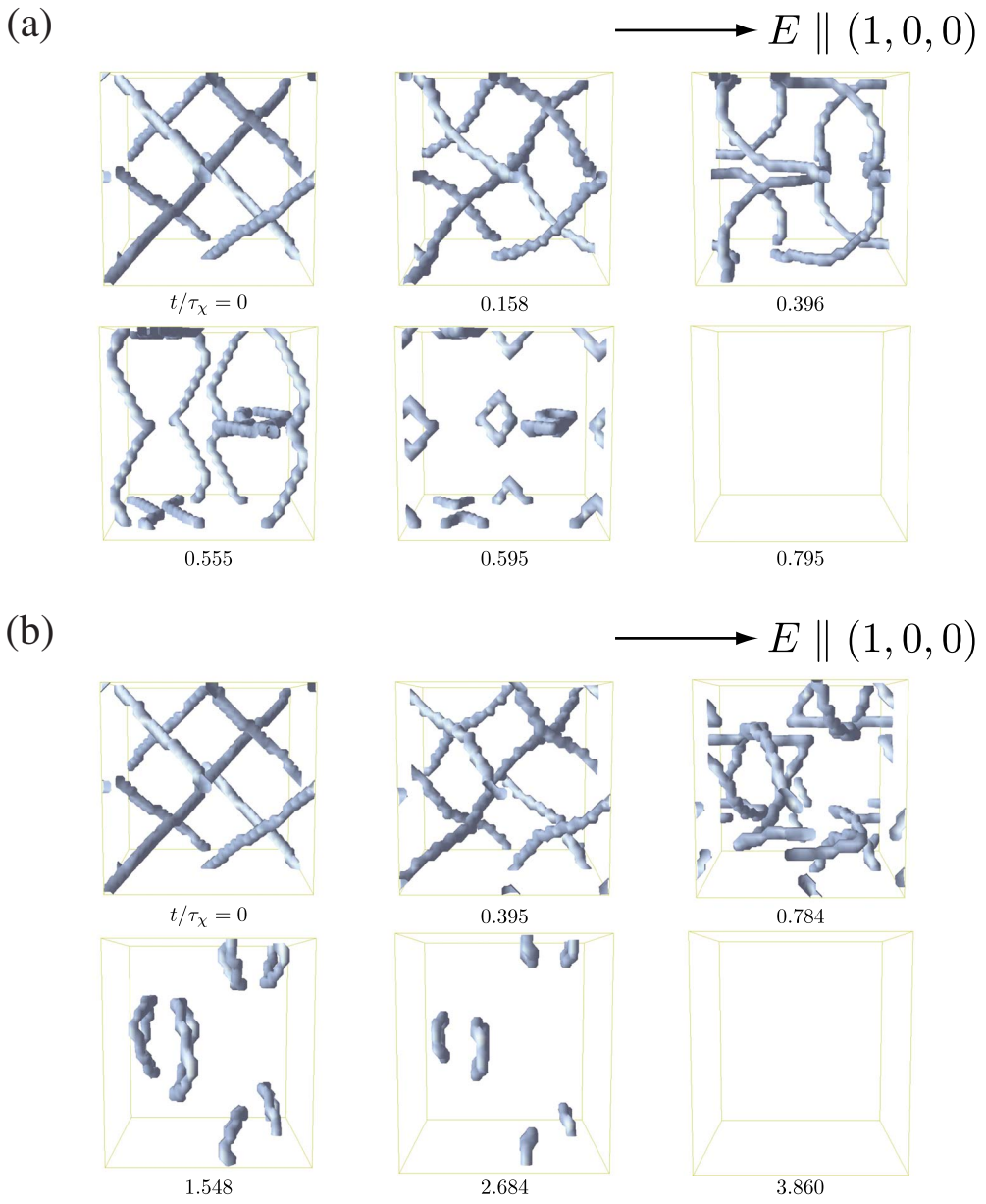

FIG. 4. (Color online) Time evolution of the O_8^- structure after the application of an electric field parallel to the [100] direction. The parameter $\bar{\epsilon}$ is (a) 5 and (b) −5. The numbers indicate the rescaled time t/τ_χ after the application of the electric field. The direction of the field is along the horizontal direction in the plane of paper as shown in the figure. We note that at t/τ_χ=0.796 in (a) and t/τ_χ=3.860 in (b), no disclination line is present and the alignment of the director is uniform along the field direction in the former, and helical in the latter.

line along the field direction appears to split into three disclination lines, as can be seen in Fig. 8(a) at t/τ_χ=0.476 (although not so clearly visible) and Fig. 9(a) at t/τ_χ =0.220. Winding of disclination lines is clearly observed in the O_8^- case [Fig. 8(a)], as in the previous calculations mentioned above. In both the O_8^- and O_2 cases, the disclination lines reorganize to form disclination rings, which again shrink and disappear to yield uniform alignment. On the other hand, when the dielectric anisotropy is negative ($\bar{\epsilon}$ <0), the disclination lines along the [111] direction remain stable throughout the relaxation process, as can be found in Figs. 8(b) and 9(b). In the O_8^- structure, other disclination lines are deformed and rearranged with topological change to result in ones parallel to the field direction [Fig. 8(b)]. A pair of junctions of disclination lines in the O_2 structure [Fig. 9(b)] move toward each other (t/τ_χ=0.275) and a bunch of four disclination lines connected at one junction point is formed (t/τ_χ=1.382). After a while, those four disclination lines are disjointed (t/τ_χ=5.809) and finally become parallel to each other and along the field direction (t/τ_χ=24.328). One important and intriguing characteristic of those kinetic processes is that the disclination lines do not disappear as in the cases discusses previously. Instead, a hexagonal array of parallel disclination lines along the field direction is formed [in Figs. 8(b) and 9(b), only one unit cell is shown. a stack of unit cells results in a hexagonal array of disclination lines]. This finding of a two-dimensional hexagonal structure might be related to the hexagonal structures arising from blue

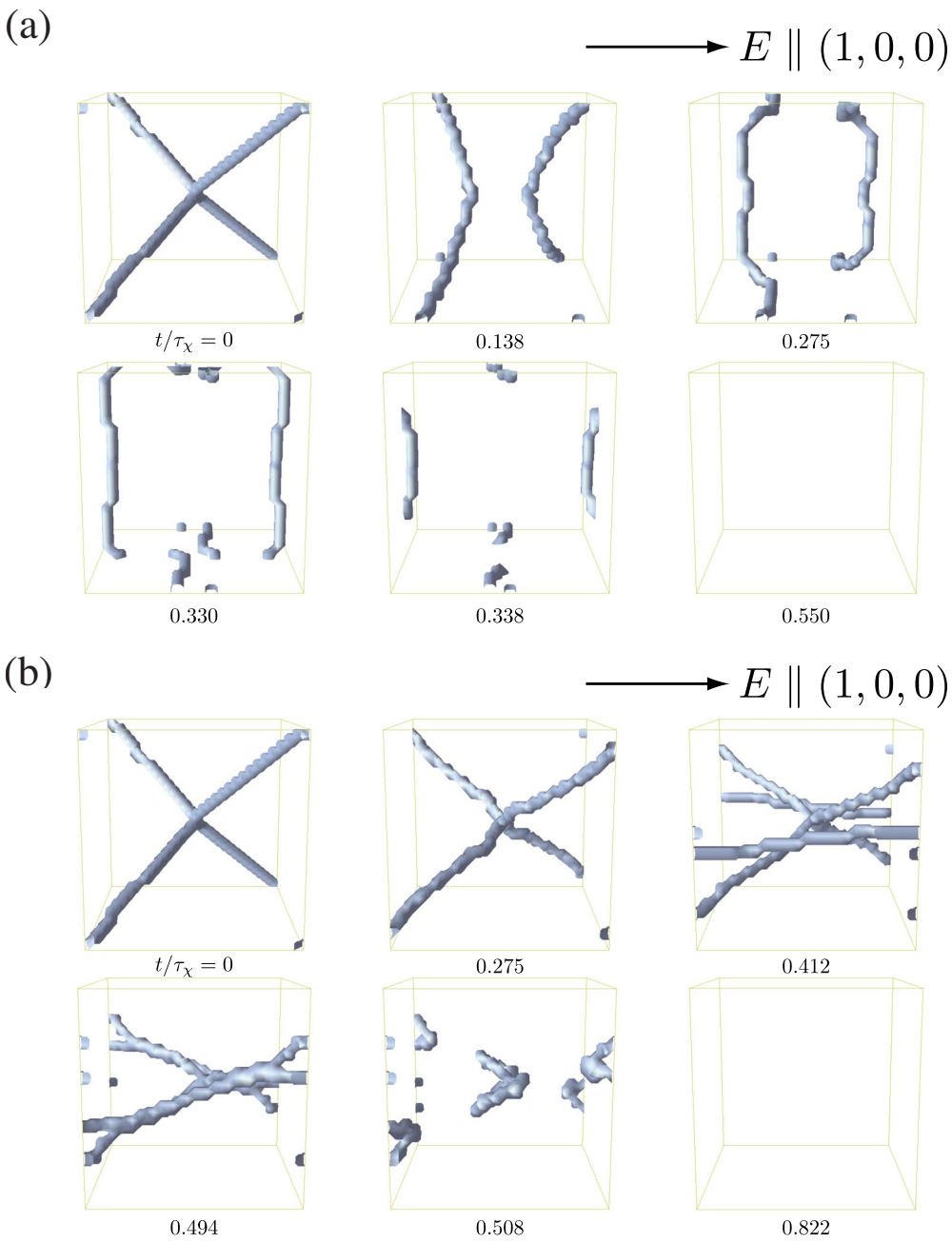

FIG. 5. (Color online) The same as Fig. 4 for the O_2 structure. Note that in (b) at t/τ_χ=0.275, two disclination lines are not connected at the center of the figure. At t/τ_χ=0.550 in (a) and t/τ_χ=0.822 in (b), no disclination line is present and the alignment of the director is uniform along the field direction in the former, and helical in the latter.

phases observed in previous experiments under an electric field [6,31,32].

Here we explain in a crude manner why a disclination line parallel to the field does not disappear when $\tilde{\epsilon}<0$. In the vicinity of a disclination line, the local director $\boldsymbol{n}$ is perpendicular to the disclination line or the electric field. When $\tilde{\epsilon}<0$, or the dielectric anisotropy is negative, $\boldsymbol{n}$ tend to be perpendicular to $\boldsymbol{E}$. Conversely, once $\boldsymbol{n}$ is perpendicular to $\boldsymbol{E}$, it is energetically stable irrespective to the direction of $\boldsymbol{n}$. Therefore, the local director $\boldsymbol{n}$ near the disclination lines experiences no torque and cannot be unstable in the presence of the electric field. As a consequence, the director field around the disclination line cannot be distorted nor rearranged by the field, which results in the stability of the disclination line along the field $\boldsymbol{E}$ when the dielectric anisotropy is negative.

Concerning the apparent splitting of the disclination along the field direction, one might wonder why a disclination of $-1/2$ strength can split. If the director $\boldsymbol{n}$ is confined in a two-dimensional plane, indeed a $-1/2$ defect cannot split into anything. However, we are dealing with a three-dimensional space, in which the topological nature of defects is different from that in two dimensions. In Fig. 10, we show the director profile at τ/τ_χ=0.476 in Fig. 8(a). Here we present the profile in a plane whose normal is along the [111] direction (or along the original disclination before splitting), and this plane is chosen so that it intersects no other discli-

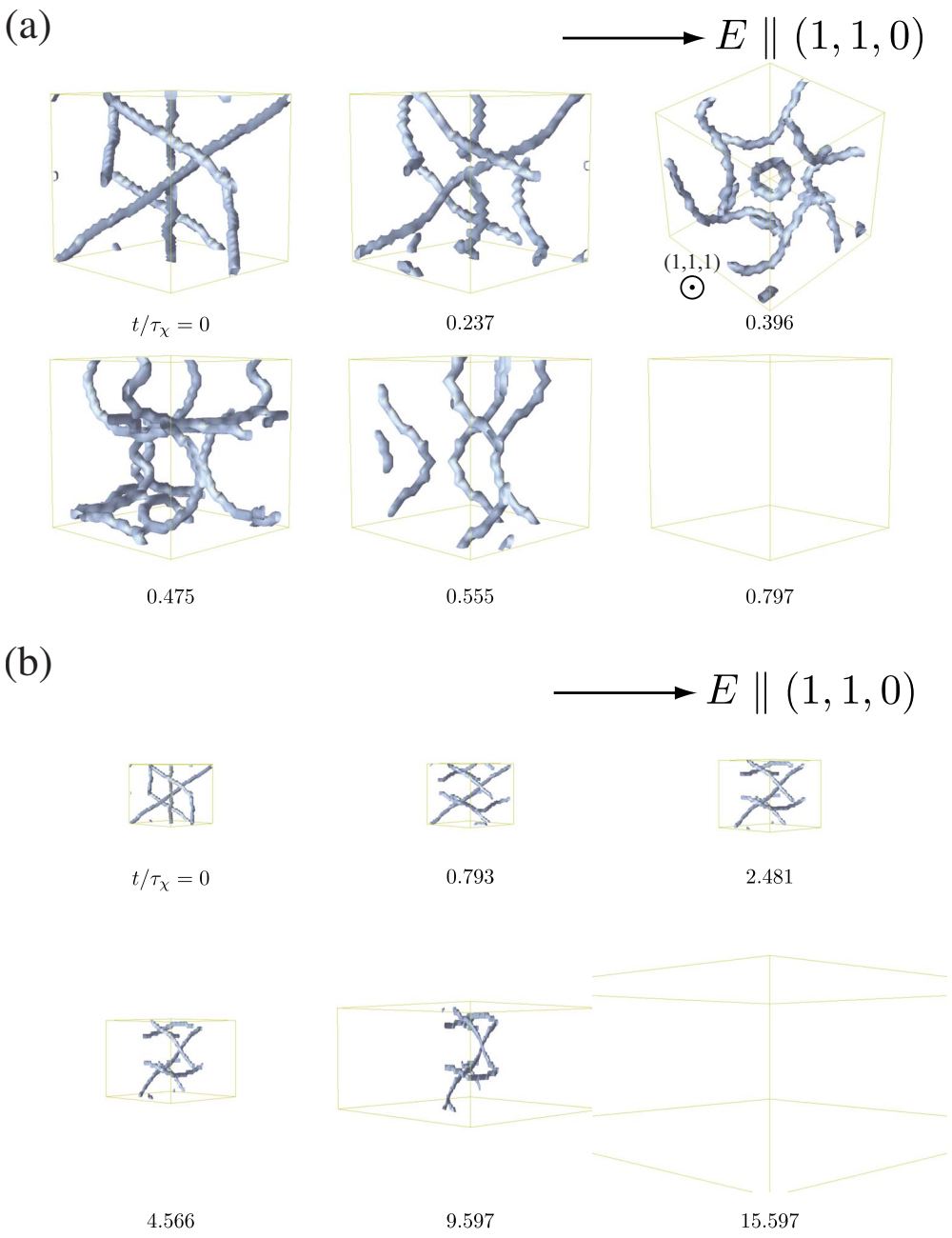

FIG. 6. (Color online) The same as Fig. 4 for the O_8^- structure with the electric field along the [110] direction. Note that in (a) at $\tau = 0.396$, the viewpoint is changed so that the [111] axis is set perpendicular to the plane of paper to make clear the winding of a disclination line that was along the [111] direction in the absence of the electric field. At $t/\tau_\chi = 0.797$ in (a) and $t/\tau_\chi = 15.597$ in (b), no disclination line is present and the alignment of the director is uniform along the field direction in the former, and helical in the latter.

nation lines than the split three disclination lines we are now interested in. Three disclinations are clearly seen in Fig. 10, and they are twist disclinations [21]. It is given in an unmistakable manner in Ref. [39] that a twist disclination, a $-1/2$ disclination, and a $+1/2$ disclination are topologically equivalent. This leads to the fact that two twist disclinations is equivalent in a topological sense to no disclinations because they can be transformed to a pair of $-1/2$ and $+1/2$ disclinations that can annihilate. Therefore, the apparent splitting of a $-1/2$ disclination line into three twist disclination lines does not break any topological rules.

To summarize this section, we have observed that in most cases, blue phases under a strong electric field transform to a uniformly aligned state (positive dielectric anisotropy), or a helical state (negative dielectric anisotropy) without any disclination lines, via complicated transformation and reorganization of disclination lines, including their winding splitting, and transformation to disclination rings. The kinetic process of the transformation of disclination lines sensitively depends on the initial structure of blue phases, direction of the electric field, and the sign of dielectric anisotropy. In a special case of negative dielectric anisotropy with the electric

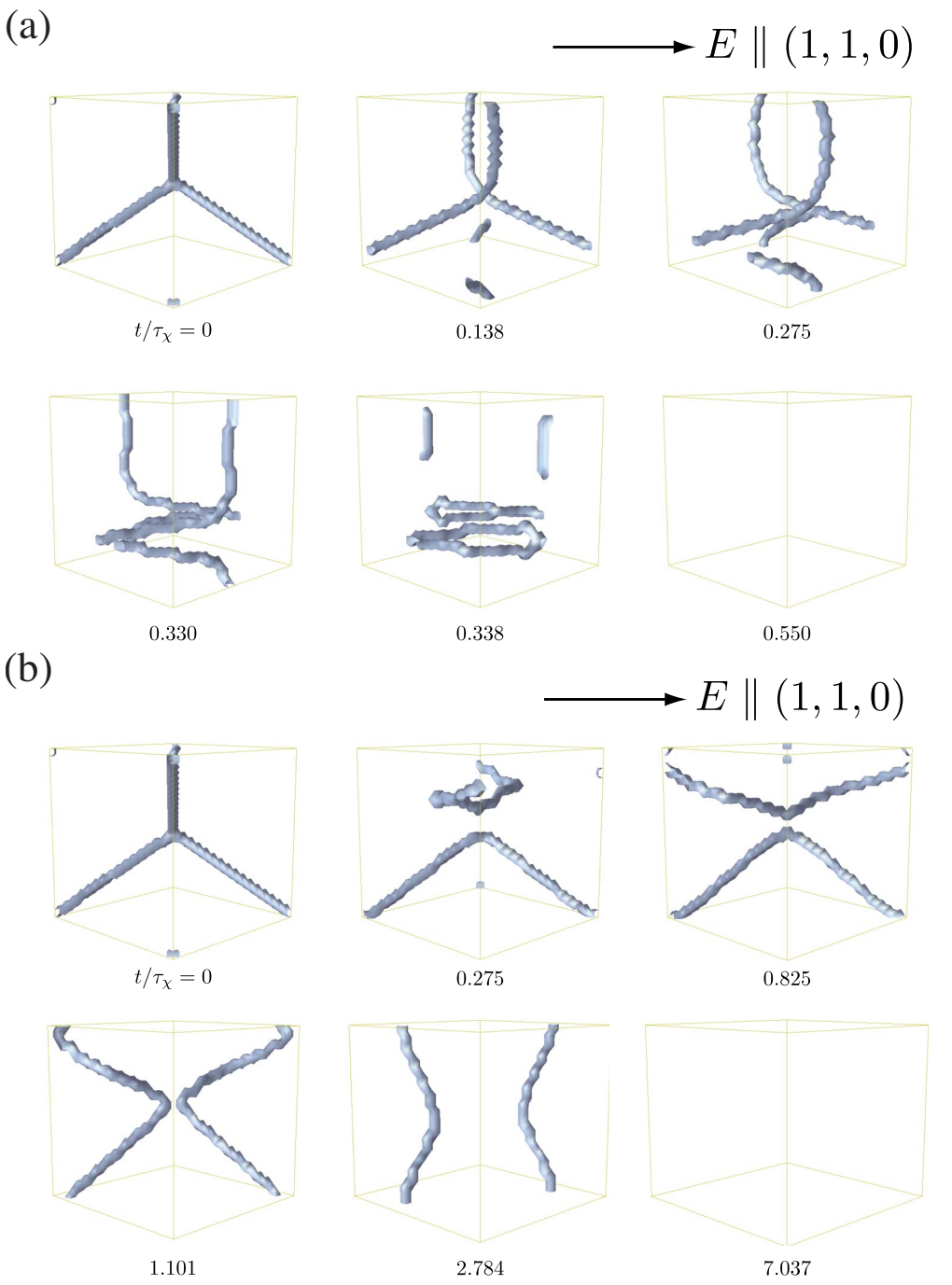

FIG. 7. (Color online) The same as Fig. 4 for the O_2 structure with the electric field along the [110] direction. Note that in (a) at t/τ_χ =0.138, two disclination lines are not connected at the center of the figure. At t/τ_χ=0.550 in (a) and t/τ_χ=7.037 in (b), no disclination line is present and the alignment of the director is uniform along the field direction in the former, and helical in the latter.

field along the [111] direction, disclination lines do not disappear and form a two-dimensional hexagonal array parallel to the electric field.

IV. CONCLUSION

We carried out a numerical study on the statics and dynamics of cholesteric blue phases. Our study is based on a Landau–de Gennes theory, in which the orientational order of a liquid crystal is taken into account by introducing a second-rank tensor order parameter. To get rid of the mismatch between the lattice parameters of the numerical system and the characteristic size of the blue phase structure minimizing the free energy and to investigate the distortion of the unit cell in response to an applied electric field, we let the size and shape of the numerical system relax by assuming simple relaxational equations for geometrical parameters characterizing the numerical system.

We investigated how the unit cell of blue phases O_8^- and O_2 is distorted under a weak and moderate electric field. We

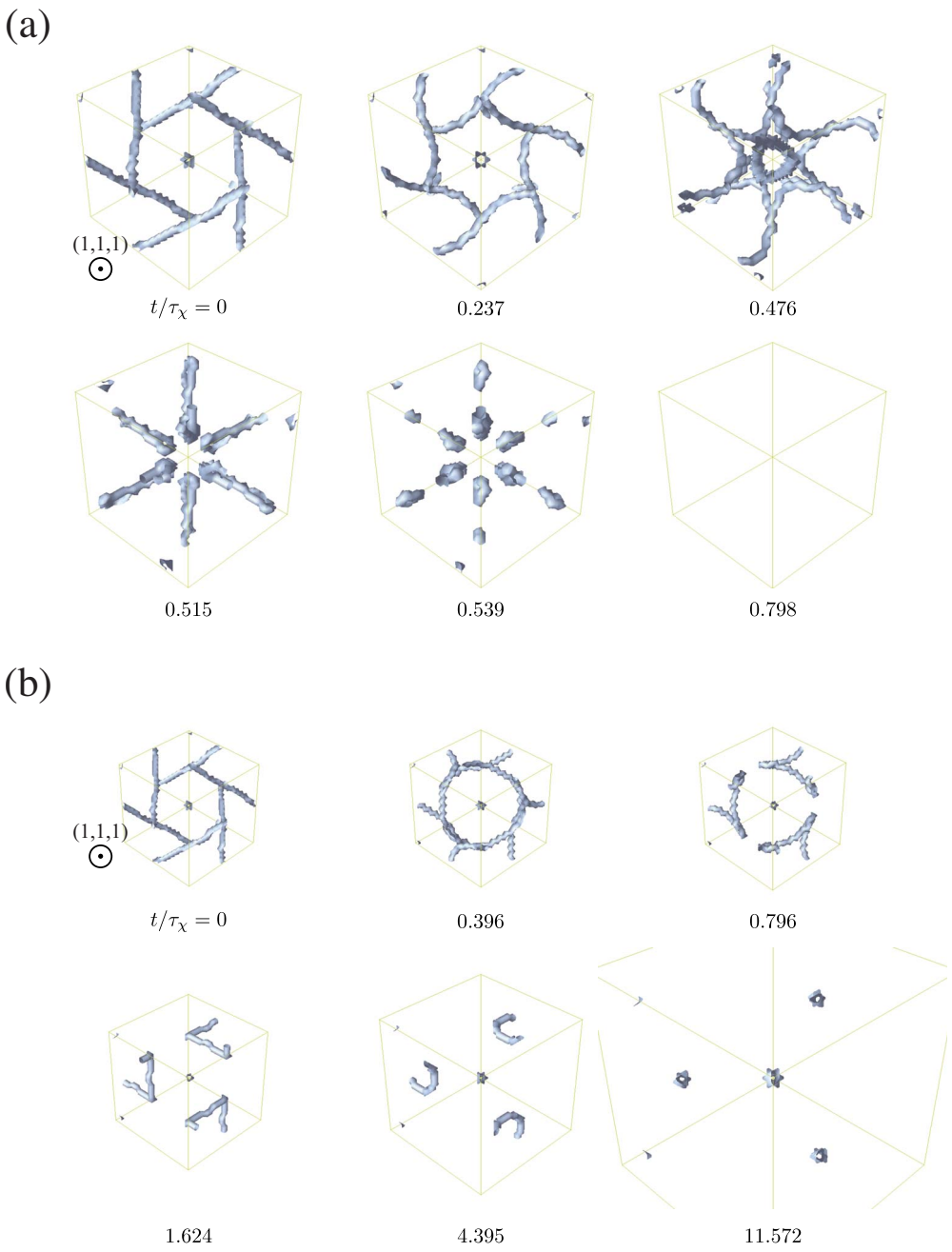

FIG. 8. (Color online) The same as Fig. 4 for the O_8^- structure with the electric field along the [111] direction. The [111] axis along the field direction is perpendicular to the plane of paper. At t/τ_χ=0.798 in (a), no disclination line is present and the alignment of the director is uniform along the field direction.

found a qualitative agreement with previous experiments in that the sign of the coefficients of the electrostriction tensor in our calculations is consistent with that determined by experiments. For a weak field, the distortion of a unit cell is well described by linear elasticity and a strain tensor expressed by a quadratic function in $\boldsymbol{E}$ [Eq. (12)]. This is confirmed by the fact that the distortion is proportional to $\tilde{\epsilon} \propto E^2$ and that the results for different field direction ([110] and [111]) give almost the same value of one of the coefficients of the electrostriction tensor R_3. For a moderate electric field, however, the distortion of a unit cell is no longer proportional to E^2, demonstrating a nontrivial response of blue phases to an electric field. This behavior of nonquadratic and nonmonotonic electrostriction reported in this paper might be detected in a more careful experiment with a larger range of the variation of E.

We also carried out calculations to see how blue phases evolve with time when a strong electric field is applied. We observed that, depending on the initial structure of blue phases (O_8^- or O_2), the direction of $\boldsymbol{E}$ and the sign of the dielectric anisotropy ϵ_a, the disclination lines in blue phase structures exhibit various complicated kinetic processes including distortion, rearrangement with topological change, and formation of disclination rings and their extinction. In

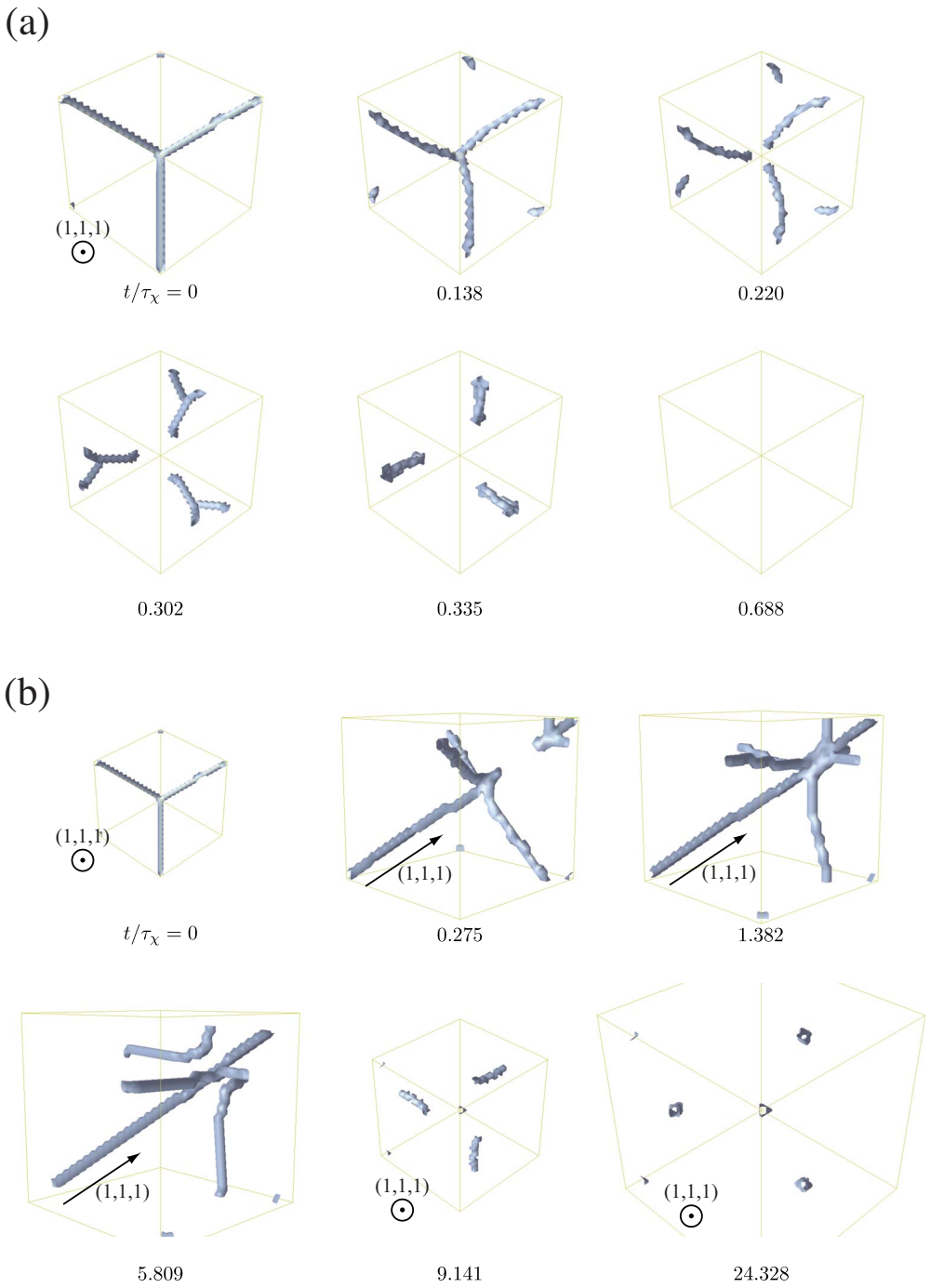

FIG. 9. (Color online) The same as Fig. 4 for the O_2 structure with the electric field along the [111] direction. In (a), the [111] axis along the field direction is perpendicular to the plane of paper. In (b), the direction of the [111] axis is indicated in each figure. Figures at t/τ_χ =0, 9.141 and 24.328 are drawn from one fixed viewpoint, and those at t/τ_χ=0.275, 1.382 and 5.809 are drawn from another fixed viewpoint. At t/τ_χ=0.688 in (a), no disclination line is present and the alignment of the director is uniform along the field direction.

most cases, the final orientational profile under a strong electric field is a uniformly aligned one for positive ϵ_a or a helical one for negative ϵ_a, and no disclination lines are present. However, when $\epsilon_a < 0$ and the field is along the [111] direction (then one of the disclination line is parallel to the field direction), disclination lines do not disappear, become parallel to the field direction, and form a two-dimensional hexagonal array.

We conclude this paper by commenting that the treatment of the time evolution of the shape and size of the unit cell together with that of an order parameter is highly difficult. Our present treatment, in which geometrical parameters characterizing the shape and size of the unit cell evolve with time via a simple relaxational equation, is one possible candidate for this problem. However, there is no guiding principle as to how to choose the characteristic time for the time evolution

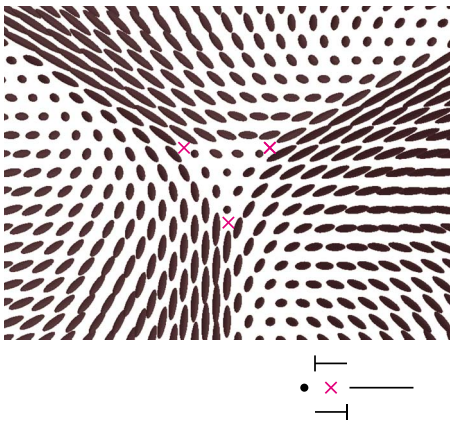

FIG. 10. (Color online) Director profile in a plane whose normal is along the [111] direction at $\tau/\tau_\chi=0.476$ in Fig. 8(a). The positions of twist disclination lines are highlighted by crosses (×). The director configuration around a twist disclination is given schematically in the nail picture.

of the unit cell [τ_Δ in Eq. (9)]. Therefore, the kinetic processes presented in Sec. III B might depend on the choice of τ_Δ, although the local reorganization processes of disclinations and orientational profiles are essentially determined by the kinetics of $Q_{\alpha\beta}$ and, therefore, we believe that the overall kinetic process is not significantly dependent on τ_Δ unless extremely small τ_Δ (fast kinetics of the unit cell) is chosen. Moreover, we did not take into account the effect of hydrodynamic flow, which, several previous numerical studies claim, might be important in the kinetics of disclination lines. So far as we know, in the field of soft materials (not restricted to liquid crystals), there has been no numerical studies based on a continuum description to simulate the time evolution of a three-dimensional ordered structure together with that of its unit cell simultaneously in a consistent manner incorporating hydrodynamics. The dynamics of cholesteric blue phases is therefore still a numerical challenge and further numerical studies are greatly encouraged.

ACKNOWLEDGMENTS

This paper was written while J.F. was staying at Department of Physics, University of Ljubljana under the support of Slovenian Research Agency (ARRS research program Grant No. P1-0099). J.F. thanks Professor Slobodan Žumer for valuable comments and kindly allowing him to finish this work. This work is supported by KAKENHI (Grant-in-Aid for Scientific Research) on Priority Area "Soft Matter Physics" from the Ministry of Education, Culture, Sports, Science and Technology of Japan.

APPENDIX A: NUMERICAL EVALUATION OF THE FREE ENERGY $\mathcal{F}$ AND ITS FUNCTIONAL DERIVATIVE $\delta\mathcal{F}/\delta\chi_{\alpha\beta}$

The discretized total free energy $\mathcal{F}$ in a unit cell is formally written as

$$\mathcal{F}=v_{\mathrm{voxel}}\sum_{i=0}^{N-1}\sum_{j=0}^{N-1}\sum_{k=0}^{N-1}\varphi_{\mathrm{voxel}}(i,j,k), \tag{A1}$$

where $\varphi_{\mathrm{voxel}}(i,j,k)$ is the (rescaled) free-energy density in a simulation voxel (i,j,k) whose volume is specified by $\boldsymbol{r}=\Sigma_{l=1}^{3}(\partial\boldsymbol{r}/\partial\xi_l)\xi_l$ with $i\le\xi_1\le i+1$, $j\le\xi_2\le j+1$, and $k\le\xi_3\le k+1$. The size of each voxel v_{voxel} is explicitly written as $v_{\mathrm{voxel}}=(\partial\boldsymbol{r}/\partial\xi_1\times\partial\boldsymbol{r}/\partial\xi_2)\cdot\partial\boldsymbol{r}/\partial\xi_3$.

We note here that φ is a function of $\chi_{\alpha\beta}$ and $\partial\chi_{\alpha\beta}/\partial r_k$. Thus, φ is regarded also as a function of $\chi_{\alpha\beta}$, $\partial\chi_{\alpha\beta}/\partial\xi_l$, and $\partial\xi_l/\partial r_k$. Since $\partial\xi_l/\partial r_k$'s are constants throughout the system as noted in Sec. II B, the free-energy density φ in the voxel (i,j,k) can be evaluated once $\chi_{\alpha\beta}$ and $\partial\chi_{\alpha\beta}/\partial\xi_l$ are known in the voxel.

For the following explanation, we define

$$\bar{\chi}_{\alpha\beta}(i,j,k)=\frac{1}{8}\sum_{i'=0}^{1}\sum_{j'=0}^{1}\sum_{k'=0}^{1}\chi_{\alpha\beta}(i+i',j+j',k+k'), \tag{A2}$$

$$\bar{\partial}_{\xi_1}\chi_{\alpha\beta}(i,j,k)=\chi_{\alpha\beta}(i+1,j,k)-\chi_{\alpha\beta}(i,j,k),$$

$$\bar{\partial}_{\xi_2}\chi_{\alpha\beta}(i,j,k)=\chi_{\alpha\beta}(i,j+1,k)-\chi_{\alpha\beta}(i,j,k),$$

$$\bar{\partial}_{\xi_3}\chi_{\alpha\beta}(i,j,k)=\chi_{\alpha\beta}(i,j,k+1)-\chi_{\alpha\beta}(i,j,k). \tag{A3}$$

Here $\chi_{\alpha\beta}(i,j,k)$ is the value of the order parameter assigned at the grid point $\{\xi_l\}=(i,j,k)$. We define the discretized version of the free-energy density using the same procedure as in Appendix A of Ref. [37] as

$$\begin{aligned}\varphi_{\mathrm{voxel}}(i,j,k)=\frac{1}{8}\sum_{i'=0}^{1}\sum_{j'=0}^{1}\sum_{k'=0}^{1}&\varphi\{\bar{\chi}_{\alpha\beta}(i,j,k),\bar{\partial}_{\xi_1}\\&\times\chi_{\alpha\beta}(i,j+j',k+k'),\bar{\partial}_{\xi_2}\chi_{\alpha\beta}(i+i',j,k+k'),\bar{\partial}_{\xi_3}\\&\times\chi_{\alpha\beta}(i+i',j+j',k)\}.\end{aligned} \tag{A4}$$

Once the equilibrium profile of $\chi_{\alpha\beta}$ is known, the total free energy $\mathcal{F}$ is calculated using Eqs. (A1) and (A4).

To evaluate the functional derivative $\delta\mathcal{F}/\delta\chi_{\alpha\beta}$, we make use of the identity [37,40]

$$\begin{aligned}\frac{\delta\mathcal{F}}{\delta\chi_{\alpha\beta}}(i,j,k)&=\frac{1}{v_{\mathrm{voxel}}}\frac{\partial\mathcal{F}}{\partial\chi_{\alpha\beta}(i,j,k)}\\&=\frac{\partial}{\partial\chi_{\alpha\beta}(i,j,k)}\sum_{i=0}^{N-1}\sum_{j=0}^{N-1}\sum_{k=0}^{N-1}\varphi_{\mathrm{voxel}}(i,j,k).\end{aligned} \tag{A5}$$

Since now the form of $\mathcal{F}$ is known as a function of a set of $\chi_{\alpha\beta}$'s, the functional derivative of $\mathcal{F}$ is readily calculated from Eq. (A5).

APPENDIX B: DERIVATION OF THE RELATION BETWEEN $\tilde{\boldsymbol{\epsilon}}$ AND $\boldsymbol{E}$

We first notice that the free-energy density f_E due to the electric field is written, in terms of the director $\boldsymbol{n}$, as [21]

$$f_E = -\frac{1}{2}\epsilon_0\epsilon_a(\boldsymbol{E}\cdot\boldsymbol{n})^2, \tag{B1}$$

in which $\epsilon_0 = 8.85\times10^{-12}$ J m^{-1} V^{-2} is vacuum permittivity, and the typical value of the dielectric anisotropy is $|\epsilon_a| \simeq 7$ [30]. If we assume a uniaxial form of the order parameter, i.e., $\chi_{\alpha\beta} = \bar{\chi}[n_\alpha n_\beta - (1/3)\delta_{\alpha\beta}]$, from Eq. (6) f_E is written in a different form as

$$f_E = -\frac{b^4}{a^3}\bar{\chi}\frac{\tilde{\epsilon}}{E^2}(\boldsymbol{E}\cdot\boldsymbol{n})^2, \tag{B2}$$

where the term independent of $\boldsymbol{n}$ has been omitted and the rescaling of the free-energy density $\varphi \equiv (a^3/b^4)f$ should be recalled.

For a and b, we use typical values given in Ref. [41], and we have $a \simeq 75\times10^3$ J m^{-3} and $b \simeq 50\times10^3$ J m^{-3}. From the precision of other parameters, we can safely set $\bar{\chi} \simeq 1$ [from Eq. (4), we have $\bar{\chi}=1.44$ for $\tau=-1$, and $\bar{\chi}=1.12$ for $\tau=-0.3$]. Since all the parameters other than $\tilde{\epsilon}$ and E^2 have been determined, we can obtain Eq. (11) by comparing Eqs. (B1) and (B2).

We also note that from the parameters above, we have $(a^2/b^3)|\epsilon_a| \simeq 2\times10^{-15}$ m^2/V^{-2}, which can be used for the estimation of the dimensional values of the components of the electrostriction tensors R_1, R_2, and R_3 in Sec. III A.

APPENDIX C: DERIVATION OF Eqs. (13)–(15)

Here we derive Eqs. (13)–(15) under the assumption of linear elasticity and Eq. (12). We note that similar calculations were carried out in Ref. [27], which focused on the spacings of the lattice planes.

We take a displacement vector $\boldsymbol{a}$ in an elastic medium with a cubic symmetry, and after deformation it is transformed to $\boldsymbol{a}'$. In the regime of linear elasticity, we have

$$|\boldsymbol{a}'|^2 = a_i a_j(\delta_{ij} + 2u_{ij}), \tag{C1}$$

where u_{ij} is the symmetric deformation tensor defined in the main text.

In the case of $\boldsymbol{E}\|[100]$, from Eq. (C1) we have

$$L_\parallel^2 = L_0^2(1+2u_{xx}),$$

$$L_\nparallel^2 = L_0(1+2u_{yy}). \tag{C2}$$

Since $\boldsymbol{E}$ is along the x direction, Eq. (12) yields $u_{xx} = R_{xxxx}E^2 = R_1E^2$ and $u_{yy} = R_{yyxx}E^2 = R_2E^2$, which leads to Eq. (13). We note that the second line of Eq. (C2) can be also written as $L_\nparallel^2 = L_0(1+2u_{zz})$, which gives an equivalent result.

When $\boldsymbol{E}$ is parallel to the [110] direction, from the definitions of $L_\parallel$ and $L_\nparallel$, we have

$$L_\parallel^2 = L_0^2(2+2u_{xx}+2u_{yy}+4u_{xy}),$$

$$L_\nparallel^2 = L_0^2(2+2u_{xx}+2u_{yy}-4u_{xy}). \tag{C3}$$

In the present case, $\boldsymbol{E} = (E/\sqrt{2}, E/\sqrt{2}, 0)$, and therefore $u_{xy} = R_{xyxy}E_xE_y = \frac{1}{2}R_3\cdot\frac{1}{2}E^2$, which results in Eq. (14).

Finally, we consider the case in which $\boldsymbol{E}$ is along the [111] direction. The definitions $L_\parallel$ and $L_\nparallel$ yield

$$L_\parallel^2 = L_0^2\left\{3+2\sum_{i=x,y,z}u_{ii}+4(u_{xy}+u_{yz}+u_{xz})\right\},$$

$$L_\nparallel^2 = L_0^2\left\{3+2\sum_{i=x,y,z}u_{ii}+4(u_{xy}-u_{yz}-u_{xz})\right\}. \tag{C4}$$

(We note that in the second line, permutations over x, y, and z give equivalent results, which reflects the threefold symmetry about the [111] axis.) Since $\boldsymbol{E} = (E/\sqrt{3}, E/\sqrt{3}, E/\sqrt{3})$, we have $u_{yz} = R_{yzyz}E_yE_z = \frac{1}{2}R_3\cdot\frac{1}{3}E^2$, and in the same manner, $u_{xz} = \frac{1}{2}R_3\cdot\frac{1}{3}E^2$. Therefore, we finally obtain Eq. (15).

[1] V. A. Belyakov and V. E. Dmitrienko, Sov. Phys. Usp. **28**, 535 (1985).
[2] H. Stegemeyer, T. Blümel, K. Hiltrop, H. Onusseit, and F. Porsch, Liq. Cryst. **1**, 3 (1986).
[3] R. M. Hornreich and S. Shtrikman, Mol. Cryst. Liq. Cryst. **165**, 183 (1988).
[4] E. Dubois-Violette and B. Pansu, Mol. Cryst. Liq. Cryst. **165**, 151 (1988).
[5] D. C. Wright and N. D. Mermin, Rev. Mod. Phys. **61**, 385 (1989).
[6] H.-S. Kitzerow, Mol. Cryst. Liq. Cryst. **202**, 51 (1991).
[7] D. L. Johnson, J. H. Flack, and P. P. Crooker, Phys. Rev. Lett. **45**, 641 (1980).
[8] P. E. Cladis, P. Pieranski, and M. Joanicot, Phys. Rev. Lett. **52**, 542 (1984).
[9] R. Barbet-Massin, P. E. Cladis, and P. Pieranski, Phys. Rev. A **30**, 1161 (1984).
[10] D. K. Yang and P. P. Crooker, Phys. Rev. A **35**, 4419 (1987).
[11] A. Saupe, Mol. Cryst. Liq. Cryst. **7**, 59 (1969).
[12] S. Meiboom, J. P. Sethna, P. W. Anderson, and W. F. Brinkman, Phys. Rev. Lett. **46**, 1216 (1981); S. Meiboom, M. Sammon, and W. F. Brinkman, Phys. Rev. A **27**, 438 (1983); S. Meiboom, M. Sammon, and D. W. Berreman, *ibid.* **28**, 3553 (1983).
[13] R. M. Hornreich and S. Shtrikman, Phys. Rev. A **24**, 635 (1981).
[14] H. Grebel, R. M. Hornreich, and S. Shtrikman, Phys. Rev. A **28**, 1114 (1983).
[15] H. Grebel, R. M. Hornreich, and S. Shtrikman, Phys. Rev. A **30**, 3264 (1984).
[16] H. Kikuchi, M. Yokota, Y. Hisakado, H. Yang, and T. Kajiyama, Nature Mater. **1**, 64 (2002).
[17] H. J. Coles and M. N. Pivnenko, Nature (London) **436**, 997 (2005).
[18] W. Cao, A. Muñoz, P. Palffy-Muhoray, and B. Taheri, Nature Mater. **1**, 111 (2002).
[19] S. Yokoyama, S. Mashiko, H. Kikuchi, K. Uchida, and T. Nagamura, Adv. Mater. **18**, 48 (2006).

[20] Seminar and Exhibition presented at the Society for Information Display (SID) 2008 International Symposium (unpublished).
[21] P. G. de Gennes and J. Prost, *The Physics of Liquid Crystals*, 2nd ed. (Oxford University Press, Oxford, 1993).
[22] A. Dupuis, D. Marenduzzo, and J. M. Yeomans, Phys. Rev. E **71**, 011703 (2005).
[23] G. P. Alexander and J. M. Yeomans, Phys. Rev. E **74**, 061706 (2006).
[24] G. P. Alexander and D. Marenduzzo, EPL **81**, 66004 (2008).
[25] A. Dupuis, D. Marenduzzo, E. Orlandini, and J. M. Yeomans, Phys. Rev. Lett. **95**, 097801 (2005).
[26] H. Stegemeyer and F. Porsch, Phys. Rev. A **30**, 3369 (1984).
[27] F. Porsch and H. Stegemeyer, Chem. Phys. Lett. **155**, 620 (1989).
[28] P. Pieranski and P. E. Cladis, Phys. Rev. A **35**, 355 (1987).
[29] N.-R. Chen and J. T. Ho, Phys. Rev. A **35**, 4886 (1987).
[30] G. Heppke, B. Jérôme, H.-S. Kitzerow, and P. Pieranski, J. Phys. (France) **50**, 549 (1989); **50**, 2991 (1989).
[31] P. Pieranski, P. E. Cladis, and R. Barbet-Massin, J. Phys. (France) Lett. **46**, 973 (1985).
[32] G. Heppke, B. Jéròme, H.-S. Kitzerow, and P. Pieranski, Liq. Cryst. **5**, 813 (1989).
[33] R. M. Hornreich, M. Kugler, and S. Shtrikman, Phys. Rev. Lett. **54**, 2099 (1985); R. M. Hornreich and S. Shtrikman, Phys. Rev. A **41**, 1978 (1990).
[34] D. Lubin and R. M. Hornreich, Phys. Rev. A **36**, 849 (1987).
[35] H. Stark and H.-R. Trebin, Phys. Rev. A **44**, 2752 (1991).
[36] L. Longa, M. Zelazna, H.-R. Trebin, and J. Mościcki, Phys. Rev. E **53**, 6067 (1996).
[37] J. Fukuda, M. Yoneya, and H. Yokoyama, Phys. Rev. E **79**, 011705 (2009).
[38] W. H. Press, S. A. Teukolsky, W. T. Vetterling, and B. P. Flannery, *Numerical Recipes*, 3rd ed. (Cambridge University Press, Cambridge, 2007).
[39] M. Kleman and O. D. Lavrentovich, *Soft Matter Physics: An Introduction* (Springer, New York, 2003), p. 454.
[40] J. Fukuda, M. Yoneya, and H. Yokoyama, Phys. Rev. E **73**, 066706 (2006).
[41] P. D. Olmsted and P. M. Goldbart, Phys. Rev. A **46**, 4966 (1992).